AIChE

Modeling of Turbulent Precipitation: A Transported Population Balance-PDF Method

Giovanni di Veroli and Stelios Rigopoulos
School of Mechanical, Aerospace and Civil Engineering, University of Manchester, Manchester M60 1QD, U.K.

DOI 10.1002/aic.12064
Published online October 28, 2009 in Wiley InterScience (www.interscience.wiley.com).

*Turbulent precipitation is a complex problem, whose mathematical description of precipitation requires a coupling of fluid dynamics with the population balance equation (PBE). In the case of turbulent flow, this coupling results in unclosed equations due to the nonlinear nature of precipitation kinetics. In this article, we present a methodology for modeling turbulent precipitation using the concept of the transported probability density function (PDF) in conjunction with a discretized PBE, simulated via a Lagrangian stochastic method. The transported PBE-PDF approach resolves the closure problem of turbulent precipitation for arbitrarily complex precipitation kinetics, while retrieving the full particle size distribution (PSD). The method is applied to the precipitation of $BaSO_4$ in a turbulent pipe flow and comparisons are made with the experimental results of Baldyga and Orciuch (*Chem Eng Sci. *2001;56:2435-2444) showing excellent agreement, while insight is drawn into the mechanisms that determine the evolution of the product PSD.* © 2009 American Institute of Chemical Engineers *AIChE J,* 56: 878–892, 2010
Keywords: turbulence, crystallization (precipitation), population balance, PDF methods, reactive flows

Introduction

Reactive precipitation is a process that involves production of particulate material via chemical reactions between reactants dispersed in a carrier fluid phase. It is a process of widespread use and industrial importance, particularly in the production of fine chemicals and pharmaceuticals, and it is also a process that poses significant challenges from the viewpoint of modeling and prediction.[1] A major objective of precipitation process design is to obtain control over the particle size distribution (PSD) of the product, as the latter often determines whether the product is suitable for particular applications, and an extensive body of research has been devoted to the development of mathematical methods for prediction of the PSD. Furthermore, in most devices of industrial importance, the flow is turbulent, and the interaction of turbulence with particle formation processes gives rise to important theoretical problems.

The evolution of the PSD is described mathematically via the population balance equation (PBE),[2] also known as general dynamic equation (GDE),[3] which is a transport equation for the distribution in a phase space comprising of space, time, and a measure of particle size (such as radius, diameter, or volume). If the particle population is polydispersed with respect to more than one variable, a multidimensional PBE can be employed.[4] Depending on the application, the PBE should contain various particle formation and interaction mechanisms that determine the evolution of the PSD—usually a combination of nucleation, growth, aggregation, and breakage*. Growth involves derivatives, while aggregation and breakage involve integrals. Therefore, when all of these mechanisms are combined, the PBE becomes an integro-differential equation. More information on the fundamentals of the PBE framework can be found on several reviews.[3,5,6]

Correspondence concerning this article should be addressed to S. Rigopoulos at stelios.rigopoulos@manchester.ac.uk

*Depending on the specific physical application, different names may be more appropriate for these mechanisms, i.e., condensation/growth, aggregation/coagulation/agglomeration, fragmentation/breakage, etc.

An extensive body of research in the solution of the PBE has been conducted. Only very simple cases can be treated with analytical methods such as the method of characteristics. The two most popular classes of methods are moment methods and discretization approaches. The former are probably the earliest and most widely employed[6,7] and are based on a representation of the PSD in terms of a finite (usually small) number of moments rather than by the full distribution. The PBE is thus transformed into a set of ODEs for these moments by integrating over the size domain. The main difficulty with the method of moments is the presence of unclosed terms in the resulting integrals, unless the kinetics assume certain simple functional forms.[7] A number of approximate moment methods have therefore been proposed; these methods are based on series expansions or on a presumed shape for the underlying PSD.[7–10] By contrast, discretization methods retrieve the full PSD and do not require any closure. Several discretization approaches exist, such as methods of classes[11,12] and finite element methods.[13–15] Finally, Monte Carlo methods[4] are often used for multidimensional PBEs. For a review of these approaches, please refer to the work of Ramkrishna.[2]

Most of these works are concerned with the solution of the PBE in spatially homogeneous domains. In actual precipitation reactors, however, or in other problems such as soot formation in combustion engines and nanoparticle production via flame synthesis, particle formation takes place within a strongly inhomogeneous flow field. These inhomogeneities can exert a profound effect on the particle formation due to the fact that particle nucleation, growth, and aggregation/breakage depend strongly on the local environment, particularly on supersaturation and shear. The next stage from the fully mixed or plug flow reactor models is to employ hybrid approaches that take some input from CFD, but still carry out the PBE calculation in a reaction engineering model.[16,17] The most detailed and accurate way of simulating precipitation in flow systems, however, is via the fully coupled CFD-PBE equations. This can be accomplished in a straightforward manner in the case of laminar flow, either via a moment-transformed or a discretized PBE.

In turbulent flows, however, random fluctuations prevent a straightforward coupling of the PBE with the Navier–Stokes equations. That is because all species concentrations and particle physicochemical processes, as well as the local PSD itself, are subject to fluctuations. As a consequence, complex nonlinear interactions arise between turbulence, chemical species transport and particle transport and formation.[3,5,18,19] Early attempts to model turbulent precipitation with CFD ignored these nonlinear interactions and proceeded by computing the turbulent flow field characteristics via a turbulence model, subsequently only considering turbulent transport (often called "mesomixing").[20] Implementation of the PBE in a CFD code, either via moments or via a discretization approach, is therefore straightforward, as is in the case of laminar flows. A consequence of this is that, even though the overall flow patterns are correctly modeled, local micromixing effects on the PBE are not being captured; these effects are more pronounced in the case of fast reactions, and precipitation reactions usually fall in this category. To take such effects into account, probability density function (PDF) methods were introduced in the turbulent precipitation literature. The essence of the PDF concept is to obtain information about the probability distribution of reactive scalars and moments or number densities, thus yielding closed forms of the nonlinear reaction/precipitation terms. In some methods, only a few parameters of the PDF (such as the mean and the variance) are being transported, and the PDF is then reconstructed by these parameters based on an assumption or interpolation; these are called presumed PDF methods, in contrast with transported or full PDF methods where the entire PDF is being transported directly.

Two main classes of presumed PDF methods have been employed in the precipitation literature. Baldyga and Orciuch, who were among the first to deal with the closure problem in precipitation, used a β-PDF for the mixture fraction in a tubular reactor,[21] in conjunction with the turbulent mixer model.[22] Apart from relying on the use of mixture fraction, the method involves a further assumption for calculating the compositions of species via linear interpolation between the nonreacting and instantaneous reaction cases. The second approach is often termed the multienvironment model (also called finite-mode PDF or DQMOM).[23,24] Piton et al.[25] initially investigated the approach for the same experimental configuration as Baldyga and Orciuch, but found significant discrepancies when comparing with their results. Others authors applied this method to different configurations,[26–28] but presented limited agreement with experimental data—in addition, no comparison was made for some important variables such as the number of particles created. Multienvironmental models, due to their coarse approximation of the PDF, may be less appropriate for cases with complex chemistry. As stressed by Fox,[29] their use with chemical kinetics that are highly sensitive to the shape of the joint PDF can be problematic for a small number of environments. In most precipitation problems, even those involving simple chemistry, homogeneous nucleation is highly sensitive to small concentrations variations.

In contrast with these two approaches, a transported PDF method does not make any assumption on the shape of the PDF. Transported PDF methods were pioneered in combustion by several researchers[30,31] and are known to be able to represent complex chemical processes. Recently, the methodology has been employed in particle formation problems such as precipitation[32] or in soot and nanoparticle formation in gas phase,[33] mostly in conjunction with the method of moments. PDF simulations are carried out either via stochastic particles, a method pioneered by Pope,[34] or via the more recent concept of stochastic fields, suggested by Valino.[35] So far, applications of PDF methods to particle formation problems have been carried out mainly with the particle method, with the exception of the work of Garmory and Mastorakos which is based on stochastic fields.[36]

In all of these attempts, the fluid dynamics were coupled with the equations for the moments of the PSD. As a result, the PSD was not directly predicted, but rather reconstructed (when needed) from its moments. The problem of reconstructing the PSD from the moments, however, is generally ill-conditioned, and no universally applicable method exists.[37] Moreover, the moment transformation results in unclosed terms except for a few special cases of growth and aggregation kernels, and some kind of closure such as Laguerre quadrature[7] or QMOM[9] is required. These methods are more or less suited

to particular problems; some comparative studies have reported that they fail to predict the correct evolution for certain kinetics, aggregation kernels or long-term behavior.[38,39]

The number of works that attempt to predict the full PSD is rather limited. Muhlenweg et al.[40] were among the first to compute the full PSD in a plug flow, neglecting micromixing effects. Nevertheless, even under this simplified conditions, they reported high-computational demands and implied that coupling with more complex CFD simulations should only be attempted when computational power has increased accordingly. Schwarzer et al.[41] considered temporal and spatial flow fluctuations using direct numerical simulation (DNS), and then employed a Lagrangian particle tracking approach to obtain the PSD. Because of the high-computational demand of DNS, their simulation was carried for very low Reynolds number only ($\sim 10^3$). As stressed by those authors, their work is useful mainly for producing reference results rather than as a viable engineering approach. Finally, Woo et al.[42] coupled a three-environment PDF with a high resolution, finite volume discretization of the PBE for growth and nucleation mechanisms. A qualitative analysis was presented, but no comparison was made with experimental results.

Recently, Rigopoulos[19] introduced a formulation for population balance modeling in turbulent flows via a discretized PBE and a transport equation for the joint PDF of species and number density. There are several advantages in this approach: the full PSD is computed directly, there is no need for closure in the PBE integral terms, and the nonlinear terms arising from the interaction of turbulence and particle formation are also closed. These features allow particle formation, growth, and aggregation/breakage mechanisms of any complexity to be incorporated. The objective of this article is to present a methodology for modeling turbulent precipitation based on the transported PBE-PDF equation by coupling a CFD code for the fluid dynamics and a Lagrangian Monte Carlo particle method to simulate the PBE-PDF. The methodology is then applied to model $BaSO_4$ precipitation in a tubular reactor, a process that is well documented in the literature and for which experimental data[21] are available for validation. The article is organized as follows: the next section briefly presents the fundamental equations of reactive flows with particle formation, outlines the need for closure in the case of turbulent flow and presents the transported PBE-PDF equation. Subsequently, the methodology for solving the transported PBE-PDF equation and coupling it with fluid dynamics is presented. This is followed by a discussion of the precipitation kinetics of $BaSO_4$, the simulation configuration and the reference experiments. The final section compares simulation results with experimental data and discusses the mechanisms underlying turbulent precipitation.

The Transported PBE-PDF Method

The fundamental equations for reactive flows with size-polydispersed particles

Problems involving polydispersed particles subject to chemical reactions, particle formation and collision/aggregation, while being transported by a carrier fluid, are described by the continuity, Navier–Stokes, species transport/reaction and PBEs. The first two, which describe the evolution of the flow field, are shown here for incompressible flow:

$$\nabla \cdot \mathbf{u}(\mathbf{x},t) = 0 \tag{1}$$

$$\frac{\partial \mathbf{u}(\mathbf{x},t)}{\partial t} + (\mathbf{u}(\mathbf{x},t)\cdot\nabla)\mathbf{u}(\mathbf{x},t) = \nu\nabla^2\mathbf{u}(\mathbf{x},t) - \frac{\nabla P(\mathbf{x},t)}{\rho} \tag{2}$$

where $\boldsymbol{u}$ is the velocity vector of the carrier fluid phase, ν the kinematic viscosity (assumed constant), P the pressure, and ρ the fluid density. For a reactive flow, where m species are being transported, these must be complemented by the species transport equation, written below in terms of the mass fractions (or concentrations) of the species involved:

$$\frac{\partial Y_a(\mathbf{x},t)}{\partial t} + \nabla(\mathbf{u}(\mathbf{x},t)\cdot Y_a(\mathbf{x},t)) = D_a\cdot\nabla^2 Y_a(\mathbf{x},t) + \dot{w}_a(\mathbf{Y},N) \qquad a = 1,m \tag{3}$$

where Y_a is the mass fraction (or concentration) of ath species, D_a is the diffusivity of Y_a, and $\dot{w}_a$ is the reactive source term for Y_a ($\dot{w}_a$ depends on the concentration array involving all species, $\boldsymbol{Y}$, as well as on the particle number density distribution, N, to be defined later). Finally, the PBE describes the evolution of the particle number density. This can be defined in terms of any characteristic property of the particles; in this work, the property of interest is a linear measure of the particle size L. Thus, the number density, $N(L;\boldsymbol{x},t)$, is a continuous distribution over the particle size domain, as well as a function of space $\boldsymbol{x}$ and time t, representing the number of particles of size L per unit L, per unit volume of space. The PBE can then be written as:

$$\frac{\partial N(L;\mathbf{x},t)}{\partial t} + \nabla(\mathbf{u}\cdot N(L;\mathbf{x},t)) + \frac{\partial}{\partial L}(G(L,\mathbf{Y})\cdot N(L;\mathbf{x},t)) = D_p\cdot\nabla^2 N(L;\mathbf{x},t) + \dot{w}_N(\mathbf{Y},N) \tag{4}$$

where, D_p is the diffusivity of the particles. The PBE introduces L as an additional dimension to the problem. Growth mechanisms are accounted for by the growth rate $G(L,\boldsymbol{Y})$ which in general, depends on the particle size and on the local environment, i.e., the concentrations of the reactive species from which the particles are grown. It can readily be seen that growth is a convective mechanism over the particle size dimension, its units being meters per second. The source term, $\dot{w}_N$, may account for particles formation (nucleation) and other phenomena such as agglomeration or fragmentation. A second additional dimension can also be added into the PBE if required (e.g., surface area for the description of particle morphology). This is particularly relevant for aggregation problems, and the solution approach presented here can be extended to accommodate multidimensional formulations. It is assumed that no slip exists between the velocity of the particles and that of the fluid phase (otherwise a distribution over velocity space would have to be considered as well). This is often the case for particles of size smaller than the Kolmogorov scale, and is appropriate for the cases considered in this article.[21]

The closure problem for the turbulent PBE and the PDF approach

In turbulent flows, the velocity field exhibits random fluctuations. As a result all transported properties, i.e., concentrations, temperature, and even size distribution, must also be considered as random variables. For engineering applications, equations for the mean values are usually

sought through a decomposition of the random variables into a mean and a fluctuating part. This procedure, known as Reynolds averaging, results in unclosed terms involving the velocity and scalar fluctuations. This issue is resolved through various closure hypotheses, which provide satisfactory answers in several flows of interest, although none of them is universally applicable. A similar closure problem is encountered by a naïve application of Reynolds averaging to the population balance, as can be readily seen later. Decomposing the instantaneous field of the number density into an average and a fluctuating part, i.e., $N = \langle N \rangle + N'$ and doing the same for the growth function, $G = \langle G \rangle + G'$ (for growth depends on the random scalar field $\boldsymbol{Y}$, and is therefore going to exhibit random fluctuations as well), we obtain for the growth term alone:

$$\left\langle \frac{\partial}{\partial L}(G \cdot N) \right\rangle = \frac{\partial \langle G \rangle \cdot \langle N \rangle}{\partial L} + \left\langle \frac{\partial G' \cdot N'}{\partial L} \right\rangle \tag{5}$$

The unclosed terms appear as a result of the nonlinearity of the growth rate ($\langle G(L,\boldsymbol{Y}) \rangle \neq G(L,\langle \boldsymbol{Y} \rangle)$), as well as a result of the correlations between number density and species' concentrations involved in the growth mechanism ($\left\langle \frac{\partial G' \cdot N'}{\partial L} \right\rangle \neq 0$). Application of the same decomposition to nucleation and aggregation results in further unknown terms. This issue is discussed in more detail by Rigopoulos.[19] In that work, a joint species-number density PDF approach was proposed to overcome the issue.

This approach proceeds as follows: at first, the number density is discretized in the size domain. The details of the discretization approach are immaterial here, and indeed any method can in principle be employed. What matters is that the distribution is approximated by a finite number of nodal values of the number density, which can be regarded as either mean values over an interval or values at finite element nodes (depending on the approach):

$$N(L;\boldsymbol{x},t) \rightarrow \{(N(L_1;\boldsymbol{x},t), N(L_2;\boldsymbol{x},t), ..., N(L_N;\boldsymbol{x},t)\}, \quad \text{or } N_i(\boldsymbol{x},t)$$

The PBE is then transformed into a number of transport equations in terms of the N_i ($N_i = N(L_i)$). These can be written as:

$$\frac{\partial N_i(\mathbf{x},t)}{\partial t} + \left(\mathbf{u}(\mathbf{x},t) \cdot \vec{\nabla}\right) N_i(\mathbf{x},t) = D_\mathrm{p} \cdot \vec{\nabla}^2 N_i(\mathbf{x},t) + \dot{W}_i(\mathbf{Y},\mathbf{N}) \quad i = 1,n \tag{6}$$

where the discretized form of the growth term has been absorbed into the new source term W_i (the functional form of which depends on the discretization scheme). It is readily seen that these equations are essentially diffusion-reaction equations similar to the species transport equations (Eq. 3).

The essence of our PBE-PDF approach is to define the joint PDF of the reactive scalars and discretized number densities, $f(\boldsymbol{y},\boldsymbol{n};\boldsymbol{x},t)$. This is to be interpreted as follows: at a point in space $\boldsymbol{x}$ and at time t, the probability that the species' mass fractions $\boldsymbol{Y}$ and the discretized number densities $\boldsymbol{N}$ simultaneously lie within the intervals ($\boldsymbol{y},\boldsymbol{y} + d\boldsymbol{y}$) and ($\boldsymbol{n},\boldsymbol{n} + d\boldsymbol{n}$), respectively, is given by $f d\boldsymbol{y}$dn. Note that we employ the standard convention of distinguishing between the instantaneous values of the fields and the sample space of the PDF by denoting the former by capital letters and the latter by lowercase.

The derivation of the transport equation for the joint PDF from Eqs. 1–3 and 6 has been shown and discussed elsewhere.[19] The final equation is:

$$\begin{aligned} \frac{\partial f}{\partial t} + \langle u_j \rangle \cdot \frac{\partial f}{\partial x_j} = & -\frac{\partial}{\partial x_j}\left[\left\langle u_j' | \mathbf{y},\mathbf{n} \right\rangle \cdot f\right] - \frac{\partial}{\partial y_\alpha}\left[\left\langle D_\alpha \nabla^2 y_\alpha | \mathbf{y},\mathbf{n} \right\rangle \cdot f\right] \\ & - \frac{\partial}{\partial y_\alpha}\left[w_\alpha(\mathbf{y},\mathbf{n}) \cdot f\right] - \frac{\partial}{\partial n_i}\left[\left\langle D_p \nabla^2 n_i | \mathbf{y},\mathbf{n} \right\rangle \cdot f\right] \\ & - \frac{\partial}{\partial n_i}\left[W_i(\mathbf{y},\mathbf{n}) \cdot f\right] \end{aligned} \tag{7}$$

The equation is written in index notation (summation over repeated indices is implied), to distinguish between the indices i, j, and α used for discretized number densities, space, and chemical species respectively, whereas space and time dependency of the variables and PDF has been omitted for sake of clarity. The terms on the left-hand side of Eq. 7 represent accumulation and convection of f by the mean flow. The first three terms on the right-hand side represent transport of f due to turbulent fluctuations, micromixing of the species' mass fractions and chemical reaction source terms. The last two terms represent micromixing of the particulate phase and any source terms due to particulate processes (any combination of nucleation, growth, aggregation, and breakage). Terms of the form $\langle X/Y \rangle$ are conditional averages, i.e., the average of the quantity X conditioned on the event Y; these terms are unknown and therefore require closure. This is a long-standing issue in the PDF literature, and an extensive body of research is available. For the turbulent diffusion term, a gradient diffusion model is commonly employed[29,43]:

$$\left\langle u_j' | \mathbf{y},\mathbf{n} \right\rangle \cdot f = -\Gamma \cdot \frac{\partial f}{\partial x_j} = -\frac{C_\mu}{Sc_t}\frac{k^2}{\varepsilon} \cdot \frac{\partial f}{\partial x_j} \tag{8}$$

where Γ is the turbulent diffusivity and C_μ and Sc_t (turbulent Schmidt number) are model constants generally taken as $C_\mu = 0.09$ and $Sc_\mathrm{t} = 0.7$ when employing a k-ε model[44]; k and ε are respectively the turbulent kinetic energy and the turbulence dissipation rate. In the above, it has been implicitly assumed that the turbulent diffusivity of the particles is the same as that of the chemical species. This is a reasonable assumption for particles smaller than the Kolmogorov length scale.[21] The closure of the micromixing terms, on the other hand, has been subject to extensive research and several models have been proposed in the literature (see Kollmann[45] for a review). One of the simplest, the Interaction via Exchange with the Mean (IEM) is employed here[46,47]:

$$\left\langle D_\alpha \nabla^2 y_\alpha | \mathbf{y},\mathbf{n} \right\rangle = \frac{1}{2\tau_\mathrm{mix}}(\langle Y_\alpha \rangle - y_\alpha) \tag{9}$$

$$\left\langle D_p \nabla^2 n_i | \mathbf{y},\mathbf{n} \right\rangle = \frac{1}{2\tau_\mathrm{mix}}(\langle N_i \rangle - n_i) \tag{10}$$

where τ_mix is a characteristic timescale of the micromixing process. The timescale τ_mix can be modeled by the following

equation, which presumes dominance of the large scale motion[29]:

$$\frac{1}{\tau_{\text{mix}}} = C_{\text{mix}} \cdot \frac{\varepsilon}{k} \tag{11}$$

where C_{mix} is a model constant generally taken equal to 2.

The source terms for both reaction and population balance in Eq. 7 are closed. All particulate processes, such as size-dependent growth, nucleation, aggregation, and fragmentation can be accommodated here. Mechanistic models of any type and complexity can be included without the need for closure assumptions; this is the main merit of the PDF formalism.

Since the dimensionality of the PDF equation is quite high [number of reactive scalars] + [number of number density nodal values] + [space, time], solution via conventional methods such as finite difference are not computationally feasible. Instead, a Lagrangian Monte Carlo method that resolves the PDF via an ensemble of notional particles will be developed here. The number of computations required by Monte Carlo methods does not scale exponentially with dimensionality, as in the case of discretization methods.

Monte Carlo simulations of the joint PDF

Lagrangian Monte Carlo methods were first introduced in the context of turbulent flows by Pope.[34] In this work, we extend the application of Lagrangian stochastic methods to simulating the PDF of the turbulent PBE. The essence of the approach is to simulate a number of stochastic entities, each one of which is equipped with its own PSD and chemical species' concentrations. The evolution of these entities is guided by the fluid dynamics, as computed by the CFD solution, as well as by stochastic equations, in such a way that their statistics approximate the sought PDF. The approach is based on the concept of equivalence between the PDF transport equation, which is essentially a Fokker–Planck type equation, and a system of Langevin-type equations for the ensemble of stochastic entities—see Gardiner[48] or van Kampen[49] for the theoretical background behind this equivalence. Accordingly, we formulate the following stochastic model for the evolution of the position, concentration (mass fractions), and PSD (discretized number density) within each stochastic particle, which is consistent with Eq. 7:

$$d\mathbf{x} = [\langle \mathbf{u}(\mathbf{x},t)\rangle + \nabla\Gamma(\mathbf{x},t)].dt + (2\Gamma(\mathbf{x},t))^{1/2}.\ d\mathbf{w} \tag{12}$$

$$dY_\alpha = \left[\frac{1}{2\cdot\tau_{\text{mix}}}(\langle Y_\alpha(\mathbf{x},t)\rangle - Y_\alpha(\mathbf{x},t)) + \dot{w}_\alpha(\mathbf{Y},\mathbf{N})\right]\cdot dt \qquad \alpha = 1,m \tag{13}$$

$$dN_i = \left[\frac{1}{2\cdot\tau_{\text{mix}}}(\langle N_i(\mathbf{x},t)\rangle - N_i(\mathbf{x},t)) + \dot{W}_i(\mathbf{Y},\mathbf{N})\right]\cdot dt \qquad i = 1,n \tag{14}$$

Equation 12 describes the motion of the notional particles in physical space due to a deterministic term and a random fluctuation introduced by $d\boldsymbol{w}$, which is the infinitesimal increment of a vector of independent Wiener processes. The discrete equivalent of a single Wiener increment during a time step Δt is $\Delta w = \Delta t^{1/2}\cdot\zeta$, ζ being a realization of a normal random variable (zero mean and unity deviation). Equations 13 and 14 describe the evolution of the stochastic particles in the phase space of the species' mass fractions and number density. This set of equations is consistent with Eq. 7 in the sense that an ensemble of entities that move and evolve according to them will feature the same statistics as the PDF of Eq. 7.

The method employed here is a hybrid Lagrangian Monte Carlo method. The flow field is computed first using conventional CFD with a RANS model for the modeling of turbulence. Subsequently, an ensemble of stochastic particles is generated, each one featuring its own concentrations of chemical species and discretized PSD. It must be stressed that these stochastic particles have no direct physical interpretation, and are certainly not to be confused with the actual particles. They are just representations of the local quantities (concentrations, number densities), in the sense that statistics of a large number of them contained in one grid cell approximates the local PDF of these quantities. The variables communicated between the CFD and the PBE-PDF solver are the mean velocities and the turbulent kinetic energy k and dissipation rate ε, which are required to compute the turbulent diffusivity Γ and time scale τ_{mix}. Motion, mixing, and precipitation are treated sequentially; this fractional step approach has been widely used in reacting flow simulations and is justified for $\Delta t << \tau_{mix}$,[29] a condition that is satisfied during our simulations.

Modeling of Turbulent Reactive Precipitation

Reactive precipitation in turbulent pipe flow

The theory will now be applied to the problem of reactive precipitation in a turbulent pipe flow, which has been studied extensively by Baldyga and Orciuch.[21] In this process reactants are injected into a liquid phase reactor, where they combine to form a solid precipitate. The particulate processes to be considered here are nucleation and growth; as stressed in Baldyga and Orciuch,[21] the concentrations of the injected species in their experiments were small enough to ensure that no aggregation is present.

Crystals are initially created when high supersaturation is generated by the forced mixing of the annular and central streams. For given initial concentrations, turbulence and mixing effects directly affect the range within which nucleation and growth can be of significant magnitude, since these depend on the local species' concentrations. In turn, the distribution of the ionic species in the reactor is determined by complex interactions of turbulent mixing and chemical reactions. The interplay of these effects will determine the PSD at the reactor outlet, which is the feature that the process engineer is most interested in. The PDF method allows for rigorous modeling of the process and closure of the nucleation and growth terms without assumptions, as well as for drawing insight into the underlying phenomena and mechanisms.

Precipitation kinetics and problem formulation

Precipitation of barium sulfate can simply be described by the following one-step reaction:

$$Ba^{2+} + SO_4^{2-} \rightarrow BaSO_4 \downarrow \quad (15)$$

At equilibrium, the quantity of precipitate is dictated by the remaining ions species whose product must be equal to the solubility (or saturation) product K_s. Before equilibrium is reached, a state of supersaturation exists where this product is higher than the final equilibrium value K_s. This state is described by the supersaturation S defined by:

$$S = \gamma \cdot \sqrt{\frac{[Ba^{2+}] \cdot [SO_4^{2-}]}{K_s}} \quad (16)$$

where $[Ba^{2+}]$ and $[SO_4^{2-}]$ are respectively barium and sulfate concentration values, and γ is the mean activity coefficient for the salt. Wei and Garside,[20] who first introduced the use of γ in this context, suggested calculating it according to the Bromley formula.[50] This approach is shared by Baldyga and Orciuch[21] as well as by much of later work.[18,28] An alternative method, based on the Pitzer approach[51] has also been reported.[52] The kinetics of barium sulfate precipitation have been extensively studied[53,54] and the dependency of nucleation and growth rates on the activity-based supersaturation S, has been derived empirically based on available experimental work.[20,21,26] However, significant discrepancies exist between the data of various authors (an example is shown in Figure 1 for the nucleation rates given by Refs. 20 and 21). Earlier expressions where the activity is not considered[55] and more theoretical approaches based on classic theory are also available.[18] The use of the latter seems limited due to the strong sensitivity of the expressions to certain parameters such as the surface tension.[18,56] For these theoretical approaches, the use of the activity-based supersaturation is essential.[18] Nevertheless, consistent results can also be obtained with a concentration-based supersaturation when employing empirical approaches, as long as the kinetic expressions have been derived in this context.[57]

In this study, we will employ the same expressions as those used by Baldyga and Orciuch, based on various experimental data. The nucleation rate, R_n, is given by:

$$R_n = R_{max,het} \cdot \exp\left(-\frac{A_{het}}{\log(S)^2}\right) + R_{max,hom} \cdot \exp\left(-\frac{A_{hom}}{\log(S)^2}\right) \quad (17)$$

where $R_{max,het} = 1.06 \times 10^{12}$ m^{-3} s^{-1}, $A_{het} = 44.60$, $R_{max,hom} = 1.50 \times 10^{45}$ m^{-3} s^{-1} and $A_{hom} = 3020$, and where the value of K_s used in Eq. 16 to calculate S here is taken as $K_s = 1.1 \times 10^{-4}$ (mol m^{-3})^2. This expression accounts for both the homogeneous and heterogeneous regimes (i.e., occurring with or without preferential sites, respectively). As it can be seen from Figure 1 (upper plot), the nucleation rate is very sensitive to the supersaturation, particularly for S higher than $\sim$500. The linear growth rate G is assumed to be size independent (McCabe's law), and is given by:

$$G = k_r \cdot \left(\gamma \cdot \sqrt{\frac{c_{1s} \cdot c_{2s}}{k_s}} - \sqrt{k_s}\right)^2 = k_d(c_1 - c_{1s}) = k_d(c_2 - c_{2s}) \quad [m/s] \quad (18)$$

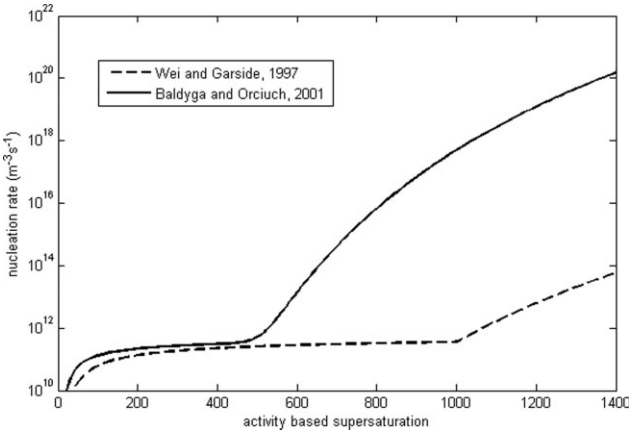

Figure 1. Plot of two different nucleation rates (from 20 and 21), both based on the experimental work of Nielsen and coworker.[53,54]

where $k_r = 3.6 \times 10^{-7}$ (m s^{-1}) (m^3 mol^{-1})^2 and k_d is the mass transfer coefficient. This expression, as well as the value of k_d, has been extensively discussed in the literature,[58,59] some authors arguing that k_d is size dependent. Baldyga and Orciuch take here a fixed value of 10^{-7} (m s^{-1}) (m^3 mol^{-1}) based on Baldyga earlier work. In the expression of G, c_1 and c_2 represent the local Ba^{2+} and SO_4^{2-} concentrations, whereas c_{1s} and c_{2s} are the concentrations of these species at the crystal surface. Since c_{1s} and c_{2s} are not directly known, Eq. 18 must be solved to get G. This was performed here by using a Newton-Raphson method.

The aforementioned approach neglects ion pair formation but gives satisfactory results because the corresponding nucleation and growth rates have been derived on the basis of this assumption. Nevertheless, some authors insisted on the importance of the ion pair (complex) $BaSO_{4(aq)}$ formation via the reaction[60]:

$$Ba^{2+}_{(aq)} + SO^{2-}_{4(aq)} \leftrightarrow BaSO_{4(aq)} \quad (19)$$

The equilibrium of Eq. 19 is described by the ion pair equilibrium constant:

$$K_{IP} = \frac{[Ba^{2+}] \cdot [SO_4^{2-}] \cdot \gamma^2}{[BaSO_{4(aq)}] \cdot \gamma_{BaSO_4}} \quad (20)$$

In Eq. 20, $[BaSO_{4(aq)}]$ stands for the concentration of the complex while γ_{BaSO_4} is the activity coefficient for this same complex; γ_{BaSO_4} can be assumed close to unity since it is a neutral species.[60] Taking into consideration the formation of this complex, Vicum et al.[52] derived new values for the parameters of the above kinetics expressions. In Eq. 17, the values $R_{max,het} = 5.36 \times 10^{11}$ m^{-3} s^{-1}, $A_{max,het} = 43.13$, $R_{max,hom} = 1.24 \times 10^{49}$ m^{-3} s^{-1} and $A_{max,hom} = 3137$ replace the previous ones, whereas $k_r = 1.02 \times 10^{-7}$ (m s^{-1}) (m^3 mol^{-1})^2 shall be used in Eq. 18. According to Ref. 60, log(Kip) $= -2.26$. For consistency, the same value of K_s is also used as recommended,[52] i.e., $\log(K_s) = -10.05$ which corresponds to $K_s = 8.91 \times 10^{-5}$ (mol m^{-3})^2. Both of these approaches (with or without ion pair) are considered in this article.

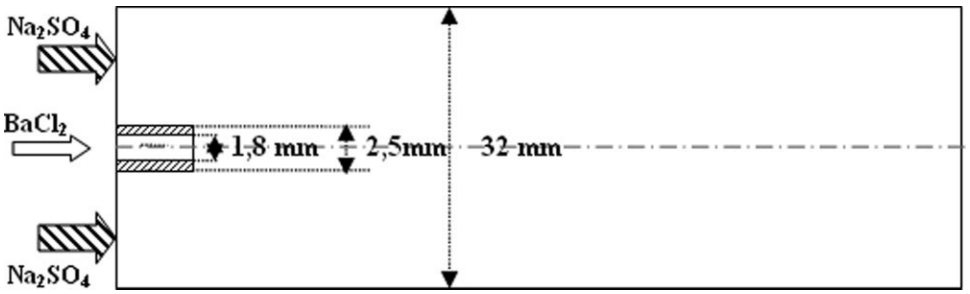

Figure 2. Geometry of the tubular reactor in the experiments of Baldyga and Orciuch[21].

The surface and volume shape factors, k_a and k_v, account for the morphology of the crystals and their values are evaluated experimentally. On the basis of previous work, Baldyga and Orciuch used $k_a = 8.17$, $k_v = 1.36$ for the low-concentration experiments (where $[BaCl_2] = 100$ mol m^{-3} is injected in the central region) and $k_a = 348.0$, $k_v = 58.0$ for the high concentration ($[BaCl_2] = 1500$ mol m^{-3} is injected in the central region). The sphericity Φ_v relates the size of the crystals to the size of spherical particles with the same volume, and is required to compare simulations and experimental results from a Coulter-counter. The value of Φ_v is given by $(\pi/(6k_v))^{1/3}$ and is equal to 0.727 and 0.208 for the low- and high-concentration experiments, respectively.

For our application, Eqs. 3 and 4 can now be written as:

$$\frac{\partial c_i(\mathbf{x},t)}{\partial t}+\nabla(\mathbf{u}\cdot c_i(\mathbf{x},t))=D_i\cdot\nabla^2 c_i(\mathbf{x},t)-k_v\frac{\rho_{BaSO_4}}{\hat{M}_{BaSO_4}}\cdot\frac{\partial m_3(\mathbf{x},t)}{\partial t} \tag{21}$$

$$\frac{\partial N(L;\mathbf{x},t)}{\partial t}+\nabla(\mathbf{u}\cdot N(L;\mathbf{x},t))+\frac{\partial}{\partial L}(G(\mathbf{Y},\mathbf{x})\cdot N(L;\mathbf{x},t))= D_{BaSO_4}.\nabla^2 N(L;\mathbf{x},t)+R_n(\mathbf{Y})\cdot\delta(L-L_0) \tag{22}$$

Equation 21 is the species transport/reaction equation written in terms of concentration. The terms ρ_{BaSO_4} and M_{BaSO_4} are the density and molar mass of $BaSO_4$ precipitate, respectively, ($\rho_{BaSO_4} = 4.48 \times 10^6$ g m^{-3} and $M_{BaSO_4} = 233.39$ g mol^{-1} at 25°C), whereas m_3 is the third moment of the size-dependent number density $N(L;\boldsymbol{x},t)$ (equal to the total volume of precipitated crystals). The last term on the right-hand side corresponds to the reactive source term and accounts for the deposition into the precipitate phase. Equation 22 is a transient and spatially distributed PBE including both nucleation and growth terms. These are related to the species' concentrations via the local supersaturation rate (Eq. 16) and the expressions given by Eqs. 17 and 18. The equilibrium with the ion pair (complex) $BaSO_{4(aq)}$ described by Eq. 20 must also be considered when using the kinetics of Vicum et al.[52]

Experimental configuration

A series of experiments of $BaSO_4$ precipitation in a tubular reactor at room temperature were reported by Baldyga and Orciuch.[21] Their configuration consisted of a main pipe (internal diameter $D_{pipe} = 32$ mm) with a concentrically located smaller pipe having external diameter $D_{nozzle\_ext} = 2.5$ mm and internal $D_{nozzle} = 1.8$ mm (Figure 2). According to Baldyga and Orciuch, both pipe lengths before injection were long enough to eliminate the entrance effects. A solution of $BaCl_2$ was injected in the central region with a concentration varying from 1500 mol m^{-3} to 100mol m^{-3} while a solution of Na_2SO_4 was injected in the outer (annular) region at a concentration of 15mol m^{-3}. The velocity ratio *Ru* (mean velocity in the injector over mean velocity in the reactor) varied from 1.0 to 6.7. Samples of the flow at the outlet were collected and the entire crystal size distribution was measured using a Coulter-counter.

Simulation setup

In our hybrid numerical approach for solving the PDF transport equation, the flow field is resolved with a conventional CFD method and the evolution of the joint species-number PDF is resolved by Lagrangian Monte Carlo particle simulation. As the flow is incompressible and the particles are assumed to have no effect on the flow field (being very small), the steady-state flow field is computed first via a CFD solver (Fluent 6.2) and subsequently an in-house developed code is employed for the Monte Carlo simulation and population balance solution. The details of both are described here.

A 2D orthogonal axisymmetric grid corresponding to the tubular reactor of Baldyga and Orciuch[21] is employed, featuring 21,000 to 50,400 nodes. The use of finer grids had no significant impact on the simulations results. The grid is refined near the injection zone, which exhibits the greatest variations. A standard k-ε turbulence model is used to compute the flow field, thus obtaining the average velocity field $\boldsymbol{u}(\boldsymbol{x})$, turbulent kinetic energy $k(\boldsymbol{x})$ and turbulent dissipation rate $\varepsilon(\boldsymbol{x})$. For each case, the inflow boundary conditions for the annular and central regions were obtained from the corresponding Reynolds number and velocity ratio. As required by the use of the wall functions approach, the near wall values of the dimensionless y^* (a grid-dependent parameter based on the turbulent kinetic energy near the walls) are ~30. Second-order upwind scheme for momentum, k and ε is employed. The standard scheme (interpolation using momentum equation coefficients) is used for the pressure while the SIMPLE scheme is used for the pressure-velocity coupling.[61] A convergence criterion of 10^{-6} is set for all residuals.

The grid as well as the data produced by the RANS simulations is then input to our in-house developed Monte Carlo

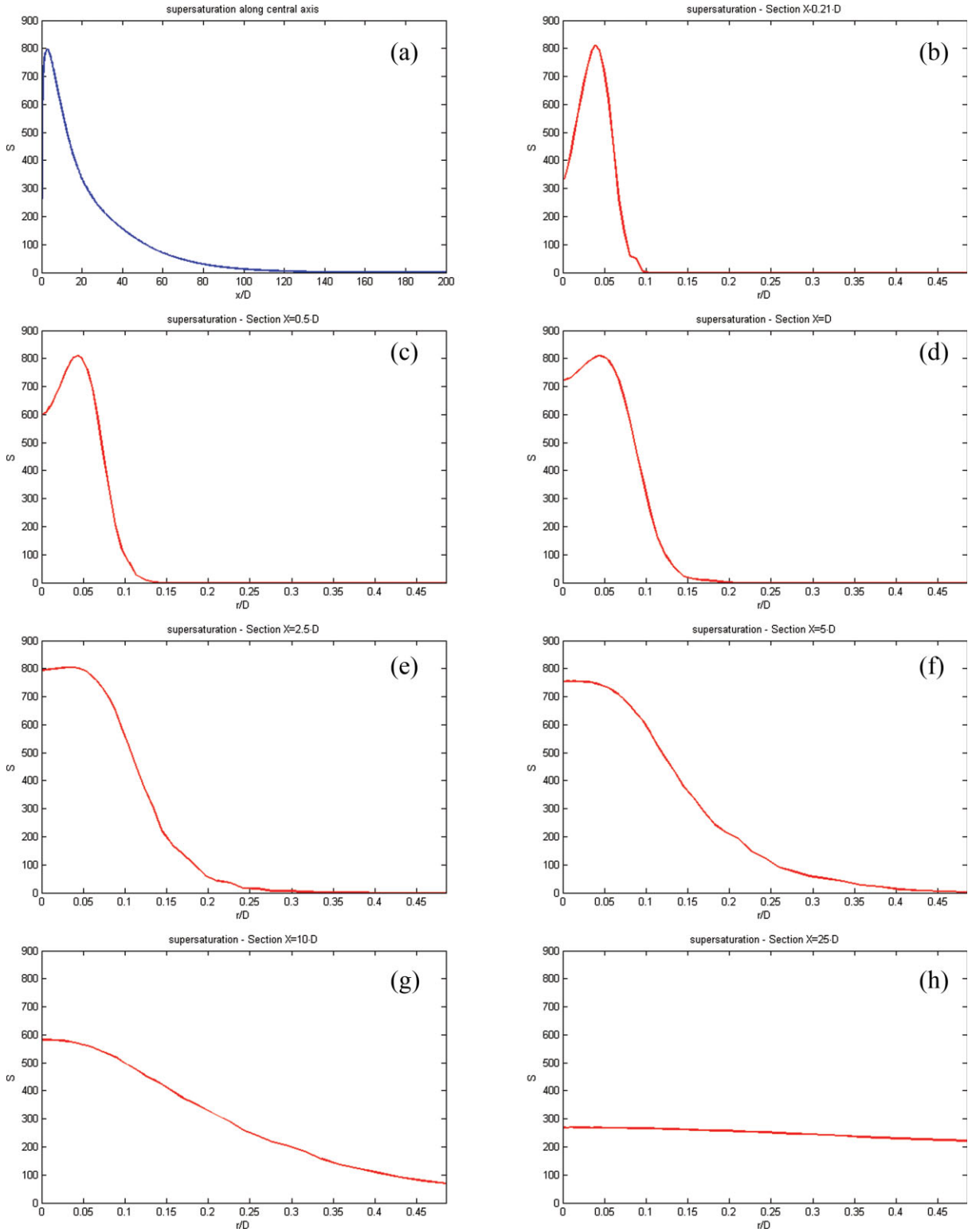

Figure 3. Supersaturation rate in the tubular reactor for Re = 30,000, c_a = 15 mol m^{-3}, c_b = 1500 mol m^{-3}, Ru = 1.

From top to bottom, left to right: (a) along central axis, (b) cross-section X = 0.21·D, (c) X = 0.5·D, (d) X = D, (e) X = 2.5·D, (f) X = 5·D, (g) X = 10·D, and (h) X =25·D. [Color figure can be viewed in the online issue, which is available at www.interscience.wiley.com.]

solver. Since no precipitation is involved before the injection of the fluid coming from the central nozzle into the main pipe, Monte Carlo simulations are not carried in the domain upstream the injection. Standard treatment of boundary conditions for the stochastic particles is implemented in the code.[29] Particles are injected at the inflow boundary

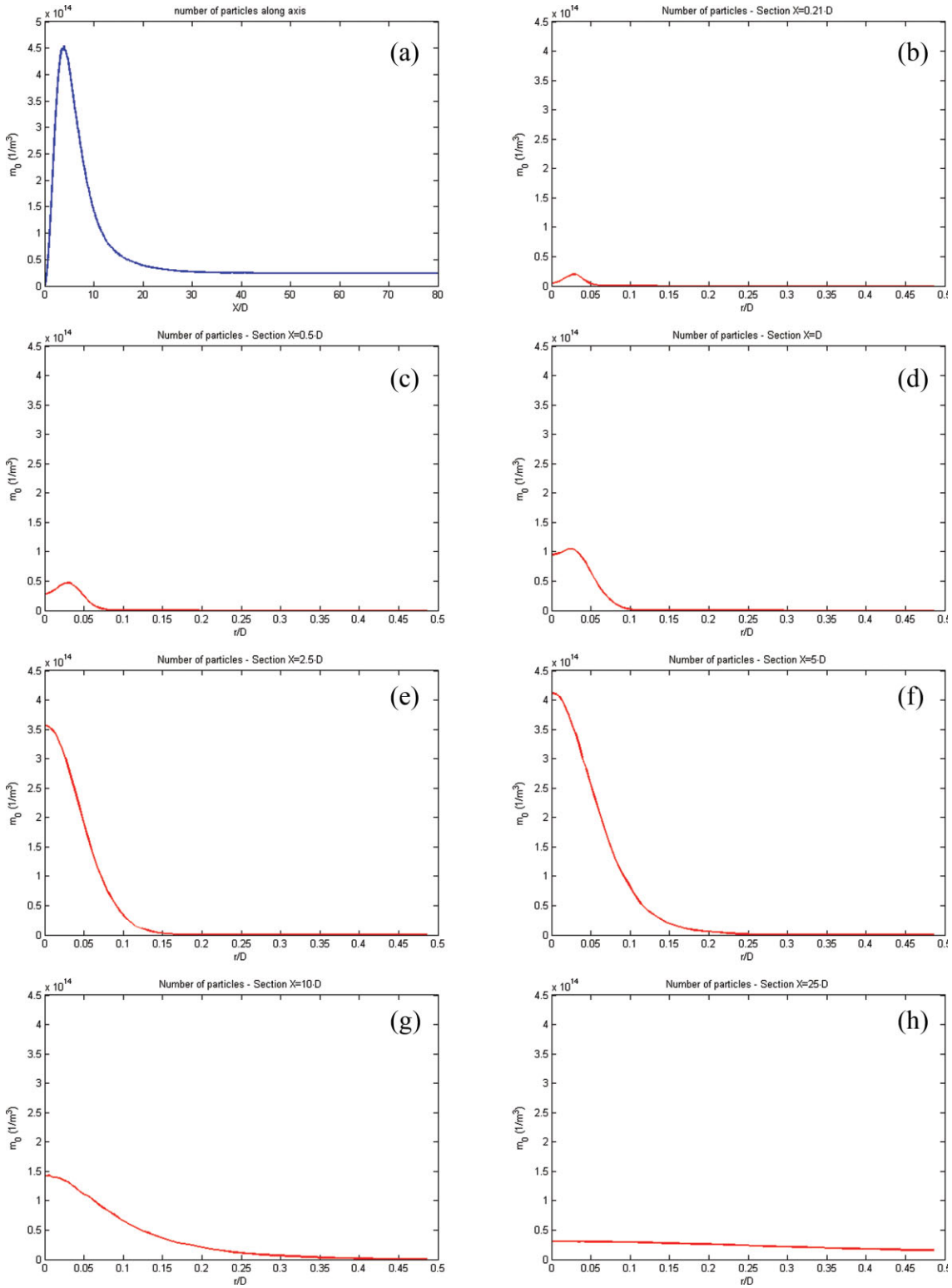

Figure 4. Number of particles per unit volume in the tubular reactor for Re = 30,000, c_a = 15 mol m^{-3}, c_b = 1500 mol m^{-3}, Ru = 1.

From top to bottom, left to right: (a) along central axis, (b) cross-section $X = 0.21{\cdot}D$, (c) $X = 0.5{\cdot}D$, (d) $X = D$, (e) $X = 2.5{\cdot}D$, (f) $X = 5{\cdot}D$, (g) $X = 10{\cdot}D$, and (h) $X = 25{\cdot}D$. [Color figure can be viewed in the online issue, which is available at www.interscience.wiley.com.]

according to the local velocity, while particles leaving the pipe at the outflow are simply deleted. Particles are reflected when crossing the central axis or the lateral wall of the pipe. Motion of the particles is governed by Eq. 12 and the local flow and turbulence characteristics. The particles injected at the inlet of the annular and central regions carry the inlet

concentration values and zero crystal number densities. To reduce the computational time requirements imposed by the CFL conditions, a local time stepping method based on particle weight corrections has been implemented in our code. The principle of this method is to use different local time steps for each cell, with appropriate modifications of particle weights.[62] The method, which can only be applied to steady-state problems, allows the simulation to converge much faster.

The scheme of Rigopoulos and Jones[15] is used to transform the number density into an equivalent discrete representation. It is a finite element method that approximates the distribution by linear functions and employs a collocation formulation for the weighted residuals. An average of 20 particles per cell has been used for all the simulations, while up to 95 scalars are carried by each stochastic particle (up to 5 chemical species + 90 nodal values for the discretized number density). Statistical errors (which are inherent in Monte Carlo simulations) were reduced by time averaging the simulations over an appropriate number of time steps[63] (the problem considered is steady state), while simulations with more particles (50–100) did not exhibit a notable improvement. The CPU time required for computations on a four-processor AMD 2.4 GHz system ranged from 12 to 22 h, indicating that solution is feasible on a desktop system.

Results and Discussion

Three experiments measuring the PSD were presented in the article of Baldyga and Orciuch.[21] We will discuss first the configuration $Re = 30{,}000$, $Ru = 1$ with the higher concentrations $c_a = 15$ mol m^{-3} and $c_b = 1500$ mol m^{-3}, which is also treated in more detail in the reference article. High-concentration experiments are generally more difficult to predict, since mixing effects are more pronounced then. Moreover, they generate large supersaturation values (here up to 800), in which case the nucleation rates are very sensible to small variations in the species concentrations (Figure 1).

In Figure 3, the cross-sectional and axial distribution of the supersaturation in the reactor are shown. A peak appears near the inlet of the central nozzle, created by the forced mixing of fluids coming from the core and annular inlets. Downstream the supersaturation is homogenized due to turbulence across the pipe radius, but also consumed due to crystal growth, hence the peak decays. The spatial distribution of the crystal concentration, i.e., the zeroth moment m_0 of the PSD (Figure 4), shows a similar trend, except that the peak is slightly transposed, indicating that a certain time is required for significant nucleation to appear. In the axial direction (Figure 4a), we can see that the peak for m_0 decays much faster than the supersaturation peak. This is mainly due to the strongly nonlinear dependence of nucleation on supersaturation, which results in nucleation being confined to a small region around the injection zone (Figure 5). Consequently m_0 is diluted within a shorter distance downstream (see, for instance, cross-sections $X = 5{\cdot}$D in Figures 3f and 4f). The mean size d_{43} of the particles, defined by $d_{43} = m_4/(\Phi_v{\cdot}m_3)$ where m_4 and m_3 are the fourth and third moments of the number density respectively and Φ_v is the sphericity, are shown in Figure 6. Unlike the zeroth moment, d_{43}

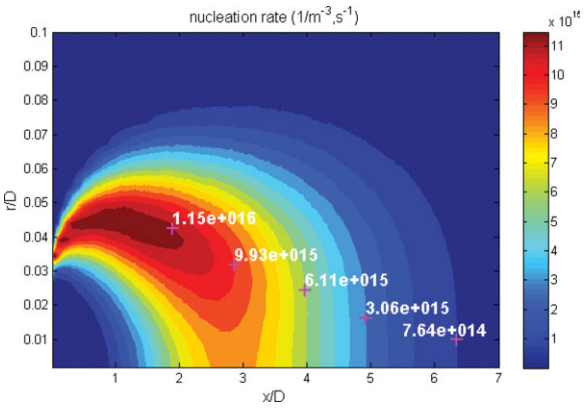

Figure 5. Contour plot of the nucleation rate near the injection zone.

[Color figure can be viewed in the online issue, which is available at www.interscience.wiley.com.]

increases along the reactor central axis at a rate similar to the decrease of supersaturation after the initial peak, i.e., it is in phase with the evolution of supersaturation. This is because the dependence of particle growth on supersaturation is not as strongly nonlinear as that of nucleation. In Figure 7, we see that the distribution of the growth rate is more uniform than that of the nucleation rate, which is limited to the area around the injection point (Figure 5). When looking at the cross-sectional distribution, d_{43} appears to be quite homogeneous within a central core that expands downstream until filling the entire cross-section (at $x \sim 2.5{\cdot}$D)—the pipe is filled with particles after this point (Figure 6).

The interplay of nucleation, growth, turbulent and mixing mechanisms, can be elucidated by investigating the evolution of the characteristic time scales of these mechanisms. As suggested by Baldyga and Orciuch,[21] the following time scale can be defined for nucleation:

$$\tau_N = \frac{m_0}{R_n} \tag{23}$$

where m_0 is the zeroth moment of the number density, also equal to the number of particles per unit volume. For growth, we can define the characteristic time scale as the ratio of the mass of the crystalline phase to the rate of the mass increase per unit time. In our case, this leads to the following expression:

$$\tau_G = \frac{M_c}{\dot{M}_c} = \frac{m_3}{3 \cdot G \cdot m_2} \tag{24}$$

where m_2 and m_3 are respectively the second and third moments of the number density and G is the growth rate as defined in Eq. 18. The micromixing timescale, which is also related to the turbulent timescale by a factor $C_{mix} = 2$, is given in Eq. 11. The profiles of τ_N, τ_G, and τ_{mix} are shown in Figure 8. From the various plots, it can be seen that nucleation is prevalent compared with growth only at the initial stage, up to $x \sim D$, in a localized area around $r \sim 0.05$ D. During this initial stage, for instance at $x = 0.21$ D, micromixing can slow down the nucleation mechanism by locally limiting the supply

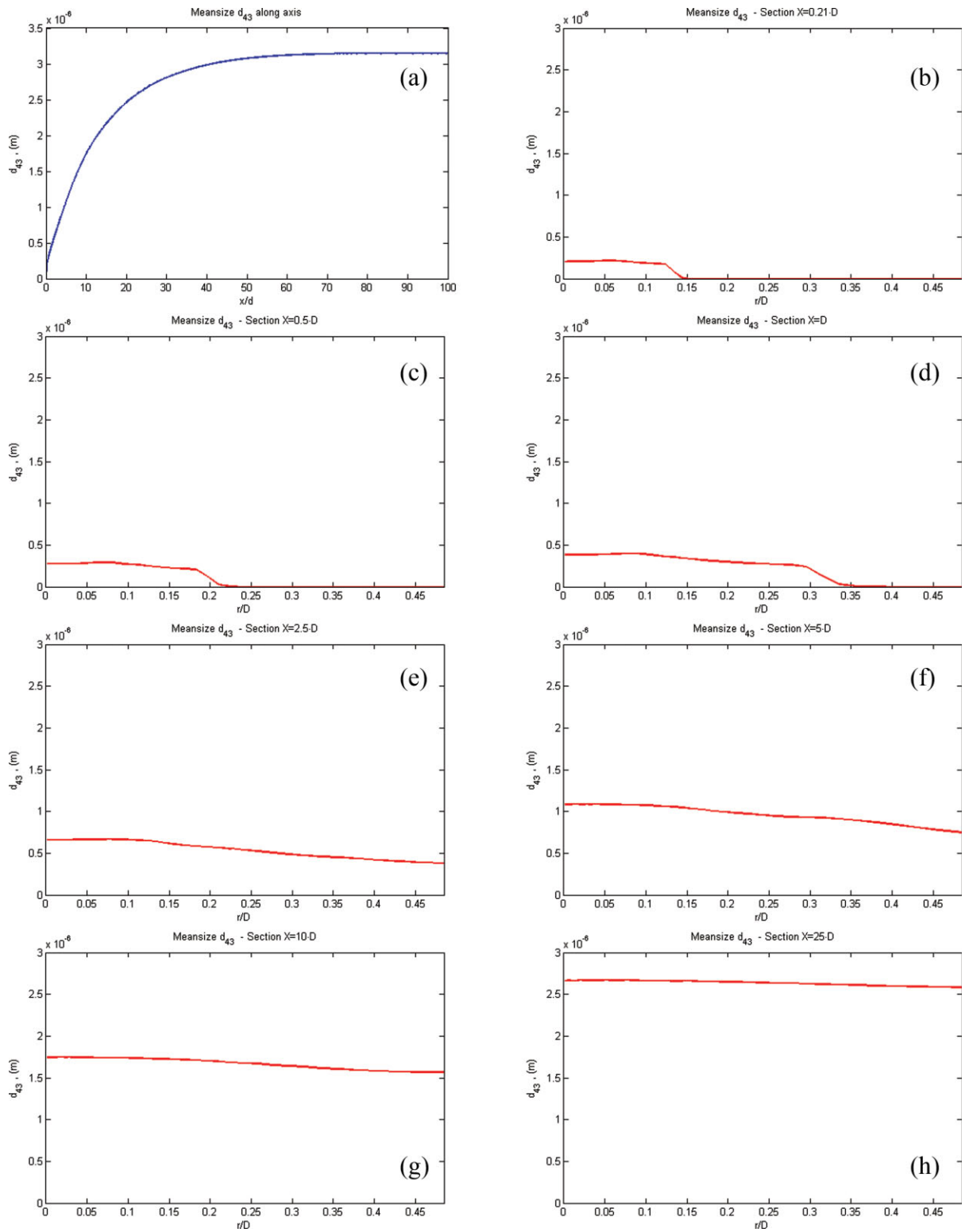

Figure 6. Mean size $d_{43} = m_4/(\Phi_v \cdot m_3)$ in the tubular reactor for Re = 30,000, c_a = 15 mol m^{-3}, c_b = 1500 mol m^{-3}, Ru = 1.

From top to bottom, left to right: (a) along central axis, (b) cross-section $X = 0.21 \cdot D$, (c) $X = 0.5 \cdot D$, (d) $X = D$, (e) $X = 2.5 \cdot D$, (f) $X = 5 \cdot D$, (g) $X = 10 \cdot D$, and (h) $X = 25 \cdot D$. [Color figure can be viewed in the online issue, which is available at www.interscience.wiley.com.]

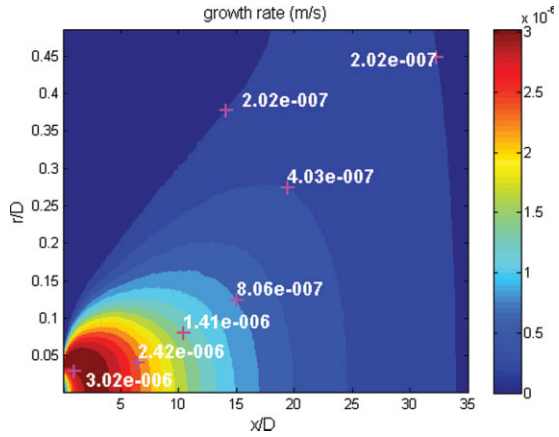

Figure 7. Contour plot of the growth rate in the first stages.

[Color figure can be viewed in the online issue, which is available at www.interscience.wiley.com.]

and homogenization of the chemical species carried by the fluid (for $r \sim 0.05$ D, $\tau_N = 10^{-3}$ while $\tau_{mix} = 8 \times 10^{-3}$); even particle growth is rather localized at this stage. Afterward, the nucleation time scale quickly increases, initially rendering nucleation secondary to particle growth ($x \sim 2.5$ D), then rather insignificant ($x \sim 10$ D). At the same time particle growth, which is now prevalent, must compete with micromixing effects within a central core that extends, for instance in the cross-section at $x = 2.5$ D, up to $r \sim 0.15$ D. Downstream, growth is slower and homogeneous across the pipe cross-sections. At this point, the micromixing time scale τ_{mix} is everywhere lower than τ_G, showing that growth is not affected any more by turbulence and micromixing effects.

A major advantage of the transported population balance-PDF method is that it retrieves directly the entire PSD. In Figure 9, the volumetric distribution is shown together with the experimental results of Baldyga and Orciuch.[21] We also plot the PSD obtained by our method with the kinetics of Vicum et al.,[52] as well as the PSD computed by Baldyga and Orciuch.[21] Since their approach does not compute the PSD directly, their PSD was reconstructed from the moments by fitting the parameters of a presumed-shape distribution (called the "most likely distribution"). The PSD obtained by the population balance-PDF method with both sets of kinetics shows excellent agreement with the experimental results, in both shape and mean size. Some minor discrepancies are expected due to both experimental error and uncertainty in kinetics. As shown in Figure 9, the mean size d_{43} is well predicted by both methods—this is expected, as it is directly related to the moments which are solved for by the method of Baldyga and Orciuch. The coefficient of variation ($=\sigma/d_{43}$) on the other hand, is much better predicted by the population balance-PDF method: it is equal to 0.25 as compared to 0.26 in the experiment, while in the PSD reconstructed from the moment method it is equal to 0.16. A slightly smaller d_{43} size is obtained with our method when implementing the kinetics of Vicum et al.,[52] but the PSD shape remains similar to the one obtained using the kinetics of Baldyga and Orciuch.[21]

Baldyga and Orciuch also reported the PSD for two other configurations: $Re = 40{,}000$, $Ru = 3$ and $Re = 40{,}000$, $Ru = 6$ with the lower concentrations $c_a = 15$ mol m^{-3} and $c_b = 100$ mol m^{-3}. Comparison of those with the results from our method using both the Baldyga and Orciuch[21] kinetics and those of Vicum et al.[52] are shown in Figures 10 and 11. For the case $Ru = 3$, the distribution obtained with our method is again close to the experimental results (Figure 10). The mean size is 3.21 μm as compared with 3.77 μm for the experiment. The two distributions have similar shape and proportions, both presenting a coefficient of variation of 0.27. For comparison, the PSD obtained by the method of moments of Baldyga and Orciuch has an average value of 3.07 μm and a coefficient of variation of 0.22. The PSD obtained with the kinetics of Vicum et al.[52] presents a lower average value of 2.84 μm, but the coefficient of variation remains correct (0.27). For the case $Ru = 6$, the agreement is slightly less satisfactory (Figure 11), the simulation yielding a mean size of 4.31 μm and a coefficient of variation of 0.26 as compared with 4.01 μm and 0.22, respectively. For comparison, the values obtained by the moments are 4.07 μm and 0.21, although the retrieved distribution looks more skewed in that case. When using the kinetics of Vicum et al.,[52] the resulting PSD shape shows better agreement with a mean size of 3.77 μm.

Conclusions

In this article, we presented a framework for modeling turbulent precipitation, based on the concept of a coupled population balance—transported PDF method,[19] by means of a Lagrangian Monte Carlo particle method coupled to a CFD code. The main advantages of the method are that: (a) it resolves the closure problem of precipitation and, more generally, of turbulent reactive flows with particles formation, (b) it allows for kinetics of arbitrary complexity (such as size-dependent growth and aggregation) to be incorporated without the need for approximations, and (c) it directly computes the entire PSD. On the other hand, like all transported PDF methods, the approach requires closure for the turbulent transport and micromixing terms, the former of which can be modeled with a gradient diffusion assumption, whereas the latter was approximated here with the simple IEM model; more sophisticated micromixing models can also be applied, and should be investigated in future studies.

The method was applied here to the precipitation of $BaSO_4$ in turbulent pipe flow and comparison was made with the experiments of Baldyga and Orciuch.[21] Results showed excellent agreement with the experimentally determined PSD in both size and shape, the latter of which is difficult to achieve with moment methods. In addition, the interplay between turbulent mixing and particle formation processes (nucleation, growth) and the competition between them was analyzed. The CPU time (12–22 h on four CPU cores) was very reasonable and showed that solution is feasible even in desktop systems.

It must be stressed that the closure problem in turbulent reactive flows with particle formation is more far-reaching than could be exemplified by the case study considered here. In particular, the $BaSO_4$ experiments featured size-independent growth and no aggregation. These features allow the

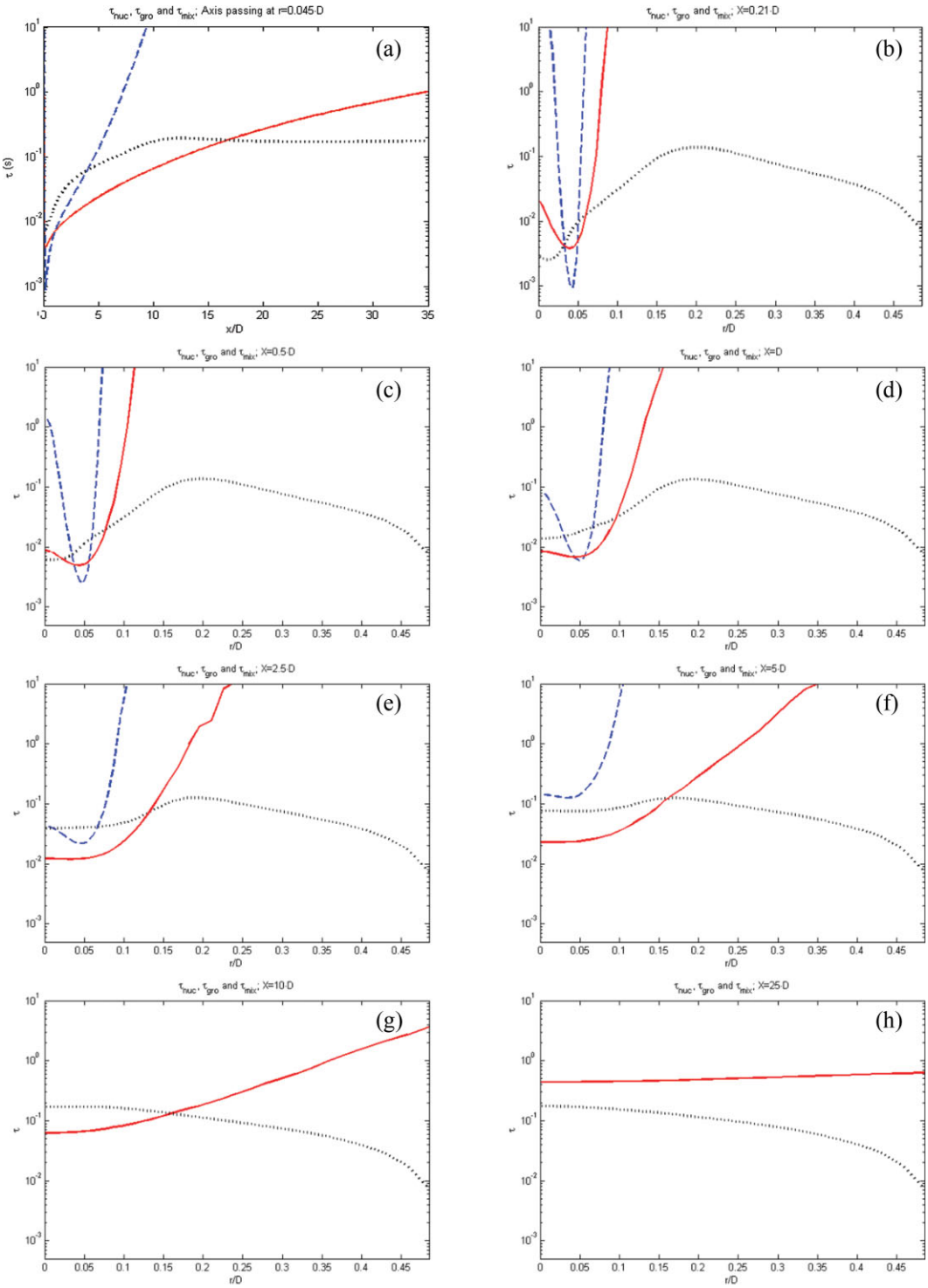

Figure 8. Characteristic time scales for nucleation, growth, and micromixing for Re = 30,000, c_a = 15 mol m^{-3}, c_b = 1500 mol m^{-3}, Ru = 1.

Broken blue line corresponds to nucleation. Solid red line corresponds to growth. Dotted black line corresponds to micromixing. From top to bottom, left to right: (a) axis passing at r = 0.05·D, (b) cross-section X = 0.21·D, (c) X = 0.5·D, (d) X = D, (e) X = 2.5·D, (f) X = 5·D, (g) X = 10·D, and (h) X = 25·D. [Color figure can be viewed in the online issue, which is available at www.interscience.wiley.com.]

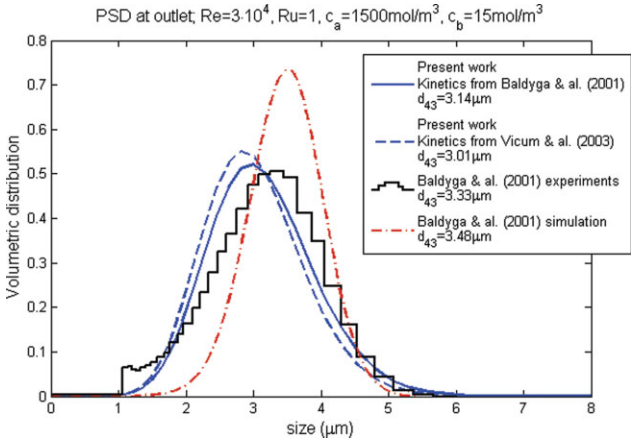

Figure 9. Particles size distribution for *Re* =30,000, c_a = 15 mol m^{-3}, c_b = 1500 mol m^{-3}, *Ru* = 1.

[Color figure can be viewed in the online issue, which is available at www.interscience. wiley.com.]

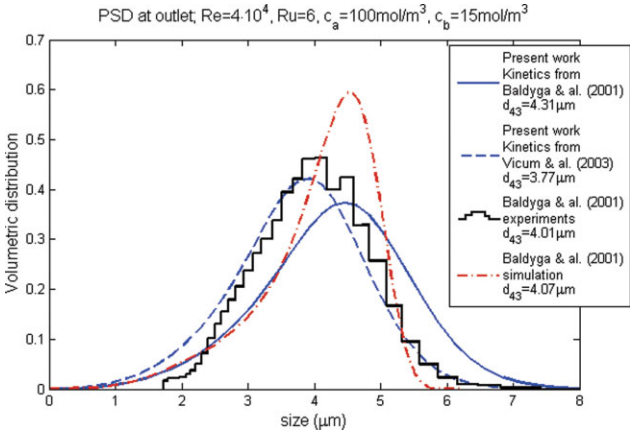

Figure 11. Particles size distribution for *Re* = 40,000, c_a = 15 mol m^{-3}, c_b = 100 mol m^{-3}, *Ru* = 6.

[Color figure can be viewed in the online issue, which is available at www.interscience.wiley.com.]

application of the method of moments, which directly computes the mean size (though not the shape of the distribution). In problems where these assumptions do not hold, unclosed integrals occur in the moment equations that require approximation (e.g., Laguerre quadrature, quadrature method of moments), while aggregation in turbulent flows results in unclosed correlations between number densities of different sizes.[3] In such problems, the advantages of the transported PBE-PDF method will be more apparent, although the simpler case considered here serves as a good benchmark due to the availability of experimental data. Future work will therefore extend the application of the method to size-dependent growth and aggregation problems. Finally, it must be emphasized that the main concept is not limited to precipitation but to any turbulent reactive flows with particle formation; as such it can be applied to a wide range of problems that exhibit similar closure issues, such as soot formation, nanoparticle production, and spray combustion.

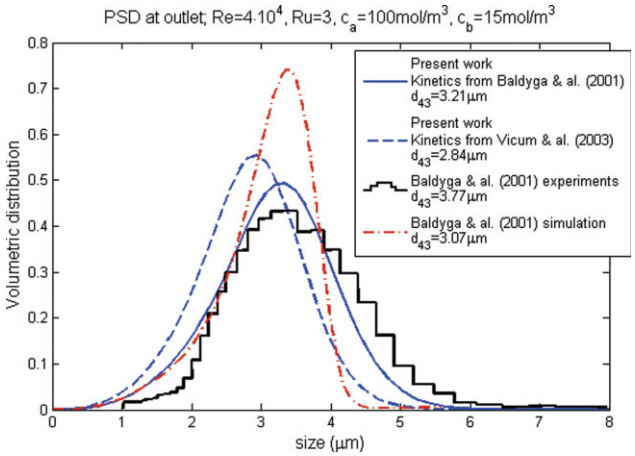

Figure 10. Particles size distribution for *Re* = 40,000, c_a = 15 mol m^{-3}, c_b = 100 mol m^{-3}, *Ru* = 3.

[Color figure can be viewed in the online issue, which is available at www.interscience.wiley.com.]

Acknowledgments

The authors gratefully acknowledge financial support by the Royal Society and by the Engineering and Physical Sciences Research Council (EPSRC) (grant EP/D079330/1).

Literature Cited

1. Sohnel O, Garside J. *Precipitation: Basic Principles and Industrial Applications*. Butterworth-Heinemann, Oxford, 1992.
2. Ramkrishna D. *Population Balances: Theory and Applications to Particulate Systems in Engineering*. New York: Academic Press, 2000.
3. Friedlander S. *Smoke, Dust and Haze: Fundamentals of Aerosol Dynamics*, *2nd ed*. New York: Oxford University Press, 2000.
4. Rosner DE, McGraw R, Tandon P. Multivariate population balances via moment and Monte Carlo simulation methods: an important sol reaction engineering bivariate example and "mixed" moments for the estimation of deposition, scavenging, and optical properties for populations of nonspherical suspended particles. *Ind Eng Chem Res*. 2003;42:2699–2711.
5. Drake RL. A general mathematical survey of the coagulation equation. In: Hidy GM, Brock JR, editors. *Topics in Current Aerosol Research. Vol. 3*, Pt. 2, Pergamon, Oxford; 1972:202.
6. Randolph AD, Larson MA. *Theory of Particulate Processes: Analysis and Techniques of Continuous Crystallization*, *2nd ed*. San Diego: Academic Press, 1988.
7. Hulburt HM, Katz S. Some problems in particle technology: a statistical mechanical formulation. *Chem Eng Sci*. 1964;19:555–574.
8. Frenklach M, Harris SJ. Aerosol dynamics modeling using the method of moments. *J Colloid Interface Sci*. 1987;118:252–261.
9. McGraw R. Description of aerosol dynamics by the quadrature method of moments. *Aerosol Sci Technol*. 1997;27:255–265.
10. Marchisio DL, Fox RO. Solution of population balance equations using the direct quadrature method of moments. *J Aerosol Sci*. 2005;36:43–73.
11. Hounslow MJ, Ryall RL, Marshall VR. Discretized population balance for nucleation, growth, and aggregation. *AIChE J*. 1988;34:1821–1832.
12. Kumar S, Ramkrishna D. On the solution of population balance equations by discretization. I. A fixed pivot technique. *Chem Eng Sci*. 1996;51:1311–1332.
13. Gelbard F, Seinfeld JH. Simulation of multicomponent aerosol dynamics. *J Colloid Interface Sci*. 1980;78:485–501.
14. Nicmanis M, Hounslow MJ. Finite-element methods for steadystate population balance equations. *AIChE J*. 1998;44:2258–2272.
15. Rigopoulos S, Jones AG. Finite-element scheme for solution of the dynamic population balance equation. *AIChE J*. 2003;49:1127–1139.

16. Zauner R, Jones AG. On the influence of mixing on crystal precipitation processes-application of the segregated feed model. *Chem Eng Sci*. 2002;57:821–831.
17. Rigopoulos S, Jones AG. Modeling of semibatch agglomerative gas-liquid precipitation of $CaCO_3$ in a bubble column reactor. *Ind Eng Chem Res*. 2003;42:6567–6575.
18. Schwarzer HC, Peukert W. Tailoring particle size through nanoparticle precipitation. *Chem Eng Commun*. 2004;191:580–606.
19. Rigopoulos S. PDF method for population balance in turbulent reactive flow. *Chem Eng Sci*. 2007;62:6865–6878.
20. Wei H, Garside J. Application of CFD modelling to precipitation systems. *Chem Eng Res Des*. 1997;75:219–227.
21. Baldyga J, Orciuch W. Barium sulphate precipitation in a pipe—an experimental study and CFD modelling. *Chem Eng Sci*. 2001;56: 2435–2444.
22. Baldyga J. Turbulent mixer model with application to homogeneous, instantaneous chemical reactions. *Chem Eng Sci*. 1989;44:1175–1182.
23. Villermaux J, Falk L. A generalized mixing model for initial contacting of reactive fluids. *Chem Eng Sci*. 1994;49:5127–5140.
24. Fox RO. On the relationship between Lagrangian micromixing models and computational fluid dynamics. *Chem Eng Process: Process Intensif*. 1998;37:521–535.
25. Piton D, Fox RO, Marcant B. Simulation of fine particle formation by precipitation using computational fluid dynamics. *Can J Chem Eng*. 2000;78:983–993.
26. Marchisio DL, Barresi AA, Fox RO. Simulation of turbulent precipitation in a semi-batch Taylor-Couette reactor using CFD. *AIChE J*. 2001;47:664–676.
27. Marchisio DL, Fox RO, Barresi AA, Garbero M. On the simulation of turbulent precipitation in a tubular reactor via computational fluid dynamics (CFD). *Chem Eng Res Des*. 2001;79:998–1004.
28. Gavi E, Rivautella L, Marchisio DL, Vanni M, Barresi AA, Baldi G. CFD modelling of nano-particle precipitation in confined impinging jet reactors. *Chem Eng Res Des*. 2007;85:735–744.
29. Fox RO. *Computational Models for Turbulent Reacting Flows*. Cambridge: Cambridge University Press, 2003.
30. Dopazo C, O'Brien EE. An approach to the autoignition of a turbulent mixture. *Acta Astronaut*. 1974;1:1239–1266.
31. Janicka J, Kolbe W, Kollmann W. Closure of the transport equation for the probability density function of turbulent scalar fields. *J Non-Equilib Thermodyn*. 1979;4:47–66.
32. Falk L, Schaer E. A PDF modelling of precipitation reactors. *Chem Eng Sci*. 2001;56:2445–2457.
33. Lindstedt RP, Louloudi SA, Pitsch H, Gore JP. Joint-scalar transported PDF modeling of soot formation and oxidation. *Proc Combust Inst*. 2005;30:775–783.
34. Pope SB. PDF methods for turbulent reactive flows. *Prog Energy Combust Sci*. 1985;11:119–192.
35. Valiño L. Field Monte Carlo formulation for calculating the probability density function of a single scalar in a turbulent flow. *Flow Turbulence Combust*. 1998;60:157–172.
36. Garmory A, Mastorakos E. Aerosol nucleation and growth in a turbulent jet using the Stochastic Fields method. *Chem Eng Sci*. 2008;63:4078–4089.
37. John V, Angelov I, Öncül AA, The'venin D. Techniques for the reconstruction of a distribution from a finite number of its moments. *Chem Eng Sci*. 2007;62:2890–2904.
38. Barrett JC, Webb NA. A Comparison of some approximate methods for solving the aerosol general dynamic equation. *J Aerosol Sci*. 1998;29:31–39.
39. Grosch R, Briesen H, Marquardt W, Wulkow M. Generalization and numerical investigation of QMOM. *AIChE J*. 2007;53:207–227.
40. Mühlenweg H, Gutsch A, Schild A, Pratsinis SE. Process simulation of gas-to-particle-synthesis via population balances: investigation of three models. *Chem Eng Sci*. 2002;57:2305–2322.
41. Schwarzer HC, Schwertfirm F, Manhart M, Schmid HJ, Peukert W. Predictive simulation of nanoparticle precipitation based on the population balance equation. *Chem Eng Sci*. 2006;61:167–181.
42. Woo XY, Tan RBH, Chow PS, Braatz RD. Simulation of mixing effects in antisolvent crystallization using a coupled CFD-PDF-PBE approach. *Cryst Growth Des*. 2006;6:1291–1303.
43. Pope SB. *Turbulent Flows*. Cambridge: Cambridge University Press, 2000.
44. Launder BE, Spalding DB. The numerical computation of turbulent flows. *Comput Methods Appl Mech Eng*. 1974;3:269–289.
45. Kollmann W. Probability density function (PDF) closures for scalar transport in turbulent flows. In: Habashi WG, Hafez MM. *Computational Fluid Dynamics Techniques, Section VII: Computational Techniques for Turbulent Flows*. Amsterdam: Gordon and Breach Publisher, 1995.
46. Villermaux J, Devillon JC. Représentation de la coalescence et de la redispersion des domaines de ségrégation dans un fluide par un modèle d'interaction phénoménologique. In: *Proceedings of the Second International Symposium on Chemical Reaction Engineering*. New York: Elsevier, 1972:1–13.
47. Dopazo C. Relaxation of initial probability density functions in the turbulent convection of scalar fields. *Phys Fluids*. 1979;22:20–30.
48. Gardiner CW. *Handbook of Stochastic Methods*, 3rd ed. Berlin: Springer, 2004.
49. van Kampen NG. *Stochastic Processes in Physics and Chemistry*, 3rd ed. Amsterdam: North-Holland Personal Library, 2007.
50. Bromley LA. Thermodynamic properties of strong electrolytes in aqueous solutions. *AIChE J*. 1973;19:313–320.
51. Pitzer K. *Activity Coefficients in Electrolyte Solutions*. Boca Raton: CRC Press, 1991.
52. Vicum L, Mazzotti M, Baldyga J. Applying a thermodynamic model to the non-stoichiometric precipitation of barium sulfate. *Chem Eng Technol*. 2003;26:325–333.
53. Nielsen AE. Nucleation and growth of crystals at high supersaturation. *Kristall Technik*. 1969;4:17–38.
54. Nielsen AE, Toft JM. Electrolyte crystal growth kinetics. *J Crystal Growth*. 1984;67:278–310.
55. Dirksen JA, Ring TA. Fundamentals of crystallization: kinetic effects on particle size distributions and morphology. *Chem Eng Sci*. 1991;46:2389–2427.
56. Lesniewski TK, Friedlander SK. Particle nucleation and growth in a free turbulent jet. *Proc Math Phys Eng Sci*. 1998;454:2477–2504.
57. Marchisio DL, Fox RO, Barresi AA, Baldi G. On the comparison between presumed and full PDF methods for turbulent precipitation. *Ind Eng Chem Res*. 2001;40:5132–5139.
58. Mersmann A. *Crystallization Technology Handbook*, 2nd ed. New York: Marcel Dekker, Inc., 2001.
59. Armenante PM, Kirwan DJ. Mass transfer to microparticles in agitated systems. *Chem Eng Sci*. 1989;44:2781–2796.
60. Monnin C. A thermodynamic model for the solubility of barite and celestite in electrolyte solutions and seawater to 200°C and to 1 kbar. *Chem Geol*. 1999;153:187–209.
61. Patankar SV, Spalding DB. A calculation procedure for heat, mass and momentum transfer in three-dimensional parabolic flows. *Int J Heat Mass Transfer*. 1972;15:1787–1806.
62. Möbus H, Gerlinger P, Brüggemann D. Comparison of Eulerian and Lagrangian Monte Carlo PDF methods for turbulent diffusion flames. *Combust Flame*. 2001;124:519–534.
63. Xu J, Pope SB. Assessment of numerical accuracy of PDF/Monte Carlo methods for turbulent reacting flows. *J Comput Phys*. 1999; 152:192–230.

Manuscript received Mar. 9, 2009, and revision received July 1, 2009.